Front. Chem. Sci. Eng. 2022, 16(11): 1606−1615
https://doi.org/10.1007/s11705-022-2200-0

RESEARCH ARTICLE

Highly hydrophobic oil−water separation membrane: reutilization of waste reverse osmosis membrane

Zihan Liu[1,2], **Yang Luo**[1,2], **Lianchao Ning**[1,2], **Yong Liu**[1], **Ming Zhang** (✉)[1,2]

1 School of Chemistry and Chemical Engineering, Tianjin University of Technology, Tianjin 300384, China
2 Center of Membrane Materials and Engineering Technology, Tianjin University of Technology, Tianjin 300384, China

Abstract The increasing applications of seawater desalination technology have led to the wide usage of polyamide reverse osmosis membranes, resulting in a large number of wasted reverse osmosis membranes. In this work, the base nonwoven layer of the wasted reverse osmosis membrane was successfully modified into the hydrophobic membrane via surface deposition strategy including TiO_2 and 1H,1H,2H,2H-perfluorooctyltrichlorosilane (PFOTS), respectively. Various techniques were applied to characterize the obtained membranes, which were then used to separate the oil–water system. The optimally modified membrane displayed good hydrophobicity with a contact angle of 135.2° ± 0.3°, and its oil–water separation performance was as high as 97.8%. After 20 recycle tests, the oil–water separation performance remained more than 96%, which was attributed to the film adhesion of the anchored TiO_2 and PFOTS layer on the surface. This work might provide a new avenue for recycling the wasted reverse osmosis membrane used in oily wastewater purification.

Keywords oil–water separation, wasted reverse osmosis membrane, hydrophobic modification

1 Introduction

The world is facing a severe water crisis as population growth and water demand exceed the conventionally available water resources [1]. In the "2020 United Nations World Water Development Report", the United Nations Educational, Scientific and Cultural Organization highlighted that the global water consumption has increased by 6 times in the past 100 years. This consumption is affected by several factors such as population growth, economic development and consumption patterns. This rate is still growing steadily at about 1% per year [2]. The pollution and the increasing shortage of drinking water resources have also pushed the quest for alternative resources, such as local and imported surface water, groundwater, desalinated brackish water, desalinated seawater and recycled water [3–5]. Membrane technology can facilitate freshwater production from all those resources [6–8]. Consequently, reverse osmosis (RO) is the most commonly used technique for desalination worldwide, primarily because of its process maturity, reliability, simplicity and current low costs. RO offers a higher water recovery and lower energy consumption than other available desalination processes [9–12]. It already accounts for 44% of the global desalination production capacity and 80% of installed desalination plants worldwide [13], with the installed capacity reaching 9.74×10^7 $m^3 \cdot d^{-1}$ in 2018 [14]. The RO membranes generally last for five to seven years [15]. Thus, the increase in the applications of RO membranes also means an increase in the disposal of water membranes. Every year, more than 840000 scrap RO membrane modules (greater than 14000 tonnes of plastic waste) are discarded in landfills worldwide [16], and this number continues to grow daily [17].

Wasted RO membranes could be used as a new resource, prolonging the potential lifespan to limit the dissemination of plastics in the environment [18]. At present, the re-use of wasted RO membranes mainly includes: i) recovery and direct re-use [6,19,20]; ii) re-use as ultrafiltration and nanofiltration membrane [21,22]; and iii) splitting and re-use as biofilm-membrane reactors, electrodialysis membrane or other uses [23–26].

The thin-film composite polyamide membrane used in most RO systems currently comprises three layers: an ultra-thin, dense, active or selective layer of aromatic polyamide (< 200 nm), a microporous support layer of polysulfone (40–60 μm), and a considerably thicker nonwoven fabric structure base made in polyester

Received May 5, 2022; accepted May 22, 2022

E-mail: zm2404@tjut.edu.cn

(~120 μm) [16,27,28]. At present, the low resistance of the RO membrane's dense selective layer to oxidants and the re-use of the skin layer account for most of the re-use of wasted RO membranes. However, these methods have complex treatment procedures and inconsistent performance after treatment because of the different types of contaminations of the epidermal layer. In fact, although the active selective layer is crucial for the RO membrane, the polyester base material, which acts as the nonwoven fabrics structure base, has a higher mass ratio. The recycling and re-use of the polyester base are essential for energy conservation and emission reduction. The polyester base material exhibits a lower degree of damage for the wasted RO membrane than the upper selective layer. Furthermore, the polyester base is easily obtained by peeling off the damaged selective layer of the wasted and dried wasted RO membrane.

As an important kind of chemical material, nonwoven fabrics are widely used in particle capture [29], material filtration [30], sewage treatment [31] and other fields. Nonwoven fabric has recently garnered popularity, especially in oil–water separation. For example, polyamide meshes and nonwoven fabrics were pre-etched using plasma and then coated by the hybrid polydopamine/cellulose to achieve highly efficient oil–water separation [32]. A gravity-driven oil–water separation using polypropylene-wood pulp fibre composite nonwoven fabric (PWNF) was also reported. PWNF develops an underwater oleophobic nature after its immersion in the deionized water for 5 min, with an underwater kerosene contact angle of 137.65° ± 4.27° [33]. Hydroxyethylcellulose and poly(acrylic acid) were selected in the research of poly(ethylene terephthalate) (PET) nonwoven fabric to form a complex membrane on the PET's surface via layer-by-layer assembly for separating water-in-oil emulsions. The membranes were further modified with thermally and chemically induced cross-linking methods, respectively, to obtain hydrophobicity. The modified membranes displayed excellent separation efficiencies with a rejection rate of more than 99.4% for all tested water-in-oil emulsions [34]. For other nonwoven fabrics, a facile and easily scaled-up approach based on thermal bonding and one-step solution immersion has been successfully developed to prepare the polypropylene/low-melt-point polyester nonwoven fabrics with high separation efficiency and oil flux. Thermal bonding by hot press and hydrophobic treatment with 1H,1H,2H,2H-perfluorodecyl-1-thiol are used to manufacture oil–water separation nonwoven fabrics, where the separation efficiency is 97%–99% and the oil flux is 62364.92 $L \cdot m^{-2} \cdot h^{-1}$ [35].

Although many studies have been conducted on oil–water separation materials, there is no report about re-using the wasted RO membrane for oil–water separation. The polyester base of wasted RO membrane re-used as oil–water separation materials was investigated in this study. This work could pave a new path for the re-use of discarded RO membranes.

2 Experiment

2.1 Materials

The polyester base material was obtained from wasted RO membranes of LCLE-4040 (RO_L, wasted RO membrane for marine use). Titanium dioxide (TiO_2, P25), petroleum ether, carbon tetrachloride, methylene blue and Sudan III were purchased from Shanghai Macklin Biochemical Co. Ltd. (China). 1H,1H,2H,2H-Perfluorooctyltrichlorosilane (PFOTS) was purchased from Aladdin Chemistry Co. Ltd. (China). Citric acid, ethanol, sodium dodecylbenzenesulfonate and sodium hyposulphite were purchased from Fuchen (Tianjin) Chemical Reagent Co. Ltd. (China). All chemicals and reagents were used as received without additional purification.

2.2 Treatment of the wasted reverse osmosis membrane

The RO_L was cut into a size of 70 mm × 50 mm. The polyester base material was obtained by directly tearing off the functional and supporting layers (Fig. S1, cf. Electronic Supplementary Material, ESM). For ultrasonic cleaning, the polyester base material was kept in a cleaning solution for 1 h (the cleaning solution comprised 3 wt % citric acid, 0.5 wt % sodium dodecylbenzenesulfonate, 0.2 wt % sodium hyposulfite and 96.3 wt % deionized water). Then, it was cleaned with deionized water and ethanol for 30 min, respectively. Finally, it was dried in an oven at 80 °C to obtain a clean polyester base material as the original membrane (M_0).

2.3 Preparation of the hydrophobic membrane

The modified membrane was prepared as follows. First, a certain amount of TiO_2 was dispersed in 400 mL of deionized water and subjected to ultrasound for 10 min. Next, the M_0 was immersed in the prepared TiO_2 solution and subjected to ultrasound for 30 min. Following ultrasonication, the membrane was soaked in the prepared TiO_2 solution for 30 min to remove any residual TiO_2 particles. Then, the membrane was removed and dried in an oven at 80 °C for 30 min to obtain a TiO_2-loaded membrane.

Second, a specific amount of PFOTS was dissolved in 400 mL of ethanol and treated with ultrasound for 10 min. Next, the TiO_2-loaded membrane was immersed in the prepared PFOTS solution and subjected to ultrasound for 30 min. It was then soaked in deionized water for 30 min to wash away the ethanol. Finally, the membrane was dried under vacuum at 80 °C for 30 min to produce a PFOTS-modified membrane (Fig. 1).

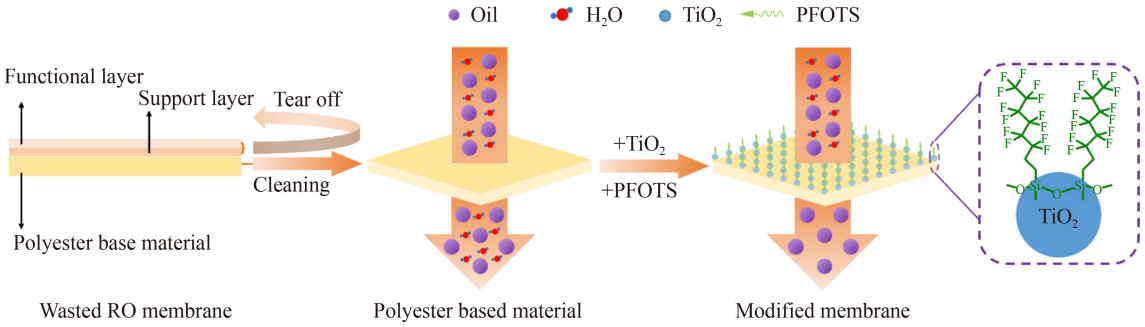

Fig. 1 Schematic illustration of the fabrication process and oil–water separation performance of the modified membrane.

2.4 Characterization

The surface morphology of prepared membranes and the elemental composition were characterized by a scanning electron microscope (SEM, ZEISS-MERLIN-Compact, Germany) equipped with an energy dispersive X-ray spectrometer (EDS) under an accelerating voltage of 5.0 kV. The contact angle (*CA*) was measured using a contact angle analyzer (SCA20, Germany) with a 2.5-μL distilled water droplet at room temperature to determine the changes in the hydrophobicity of the membrane surface. The *CA* value of each membrane was the average of five independent measurements. The chemical composition in each sample was evaluated via Fourier-transform infrared spectroscopy (FTIR, STA6000-TL9000-MS, USA) and X-ray photoelectron spectroscopy (XPS, ESCALAB250Xi, UK). The FTIR spectra were collected at a scanning range of 4000–400 cm^{-1} by cumulating 20 scans at ambient temperature with a resolution of 2 cm^{-1}.

2.5 Separation performance evaluations

The membrane was fixed on the separation equipment having a diameter of 40 mm. Oil (carbon tetrachloride) was poured into the separation equipment equipped with a different membrane. The oil flux (F_o) of the membrane was calculated from the following equation:

$$F_o = \frac{V_o}{A \times T}, \tag{1}$$

where V_o is the oil volume (L), A is the effective filtration area of membrane (m^2) and T is the permeation time (h).

The oil–water mixtures (30:70, v/v) were poured into the separation equipment, and the separation test was conducted by gravity alone to compare the oil/water separation efficiency among different membranes. Carbon tetrachloride was used as the oil phase in this experiment. The separation efficiency (R_o) of the membrane was calculated as follows:

$$R_o = \frac{m_1}{m_0} \times 100\%, \tag{2}$$

where m_0 is the weight of oil (g) in the feed and m_1 is the weight of oil in the filtrate (g).

After the filtration process, the tested membrane was placed in an oven at 80 °C for drying. It was then re-used for the subsequent oil–water separation. The flux recovery rate was used to evaluate the membrane's stability. The flux recovery rate (*FRR*) was calculated as follows:

$$FRR = \frac{F_n}{F_0} \times 100\%, \tag{3}$$

where F_0 is the first tested oil flux ($L \cdot m^{-2} \cdot h^{-1}$) and F_n is the nth tested oil flux ($L \cdot m^{-2} \cdot h^{-1}$).

3 Results and discussion

3.1 Analysis of orthogonal experiments

The separation performance of the modification membrane is closely related to preparation conditions such as mass concentration of TiO_2, the volume concentration of PFOTS, and the deposition times of TiO_2 and PFOTS. An orthogonal experiment was designed to determine the optimal preparation conditions of modification by investigating the effects of preparation conditions on separation performance. The optimal conditions were determined by analyzing the CA, oil flux and oil–water separation efficiency. Table 1 presents the results of the orthogonal experiment. Table 2 shows the testing indexes. Four factors with three levels involving nine membranes are present. These four factors are the mass concentration of TiO_2 (C_T), TiO_2 deposition time (t_1), the volume concentration of PFOTS (C_P) and PFOTS deposition time (t_2). The testing indexes are the water contact angle *CA*, oil flux F_o, and oil–water separation efficiency R_o.

Table 2 also presents the results of the orthogonal analysis, which is shown as follows. Figures S2 and S3 (cf. ESM) present the detailed data of the orthogonal experiment. When the *CA* was used as the testing index, the priority of preparation conditions was expressed as $C_T > t_1 > t_2 > C_P$, corresponding to the optimal preparation conditions of 0.25 $g \cdot L^{-1}$, 15 min, 0.75 $mL \cdot L^{-1}$ and 10 min, respectively. When F_o was used as the testing

Table 1 Programme of the orthogonal experiment

Membrane number	Factor				Index		
	C_T/ (g·L^{-1})	t_1/ min	C_P/ (mL·L^{-1})	t_2/ min	CA/ (°)	F_o/ (L·m^{-2}·h^{-1})	R_o/ %
M_1	0.125	5	1.00	5	108.7	236.14	97.9
M_2	0.125	10	0.50	10	125.8	237.36	97.6
M_3	0.125	15	0.75	15	129.7	231.48	97.5
M_4	0.250	5	0.75	10	131.6	190.24	97.2
M_5	0.250	10	1.00	15	133.3	184.98	97.4
M_6	0.250	15	0.50	5	134.3	192.62	97.9
M_7	0.500	5	0.50	15	125.8	193.32	99.3
M_8	0.500	10	0.75	5	128.7	188.67	98.2
M_9	0.500	15	1.00	10	134.1	170.27	95.6

Table 2 Results of the orthogonal experiment

Index	Parameter	C_T	t_1	C_P	t_2
CA	K1	121.4	122.0	125.4	123.9
	K2	133.1	129.3	128.6	130.5
	K3	129.6	132.7	130.0	129.6
	R	11.7	10.7	4.6	6.6
	Priority	$C_T > t_1 > t_2 > C_P$			
F_o	K1	234.99	206.56	197.13	205.81
	K2	189.28	203.67	207.77	199.29
	K3	184.09	198.12	203.46	203.26
	R	523.14	12.27	19.09	7.20
	Priority	$C_T > C_P > t_1 > t_2$			
R_o	K1	97.67	98.13	98.27	98.00
	K2	97.50	97.73	97.63	96.80
	K3	97.70	97.00	96.97	98.07
	R	0.20	1.13	1.30	1.27
	Priority	$C_P > t_2 > t_1 > C_T$			

index, the priority was expressed as $C_T > C_P > t_1 > t_2$, corresponding to the optimal conditions of 0.125 g·L^{-1}, 5 min, 0.75 mL·L^{-1} and 5 min, respectively. When R_o was used as the testing index, the priority was presented as $t_2 > C_P > t_1 > C_T$, corresponding to the optimal conditions of 0.500 g·L^{-1}, 5 min, 0.50 mL·L^{-1} and 15 min, respectively. The oil flux in each run of the experiment was more than 170 L·m^{-2}·h^{-1}, and the gap between each other was within 100 L·m^{-2}·h^{-1}. This finding shows that the preparation conditions exerted a little effect on the oil flux. Similarly, the oil–water separation efficiencies in each run of experiments were all above 95%, suggesting a slight influence of preparation conditions on the separation efficiencies. Finally, the *CA* was determined to be used as the testing index.

The SEM results of modified membrane M_1–M_9 (Fig. 2) reveal that the surface of the modified membrane gradually shows particle aggregation and gradually becomes rough with the increasing mass concentration of TiO_2. There were few particles on the membrane when the mass concentration of TiO_2 was 0.125 g·L^{-1} (Fig. 2 (M_1, M_2, M_3)). When the mass concentration of TiO_2 added to the reaction solution was increased to 0.25 g·L^{-1} (Fig. 2 (M_4, M_5, M_6)), the TiO_2 particles on the membrane were also increased. In addition, the membrane surface showed a uniform and dense distribution of TiO_2 particles. When the mass concentration of TiO_2 increased to 0.5 g·L^{-1} (Fig. 2 (M_7, M_8, M_9)), the TiO_2 particles on the membrane increased significantly and began to accumulate, and the surface

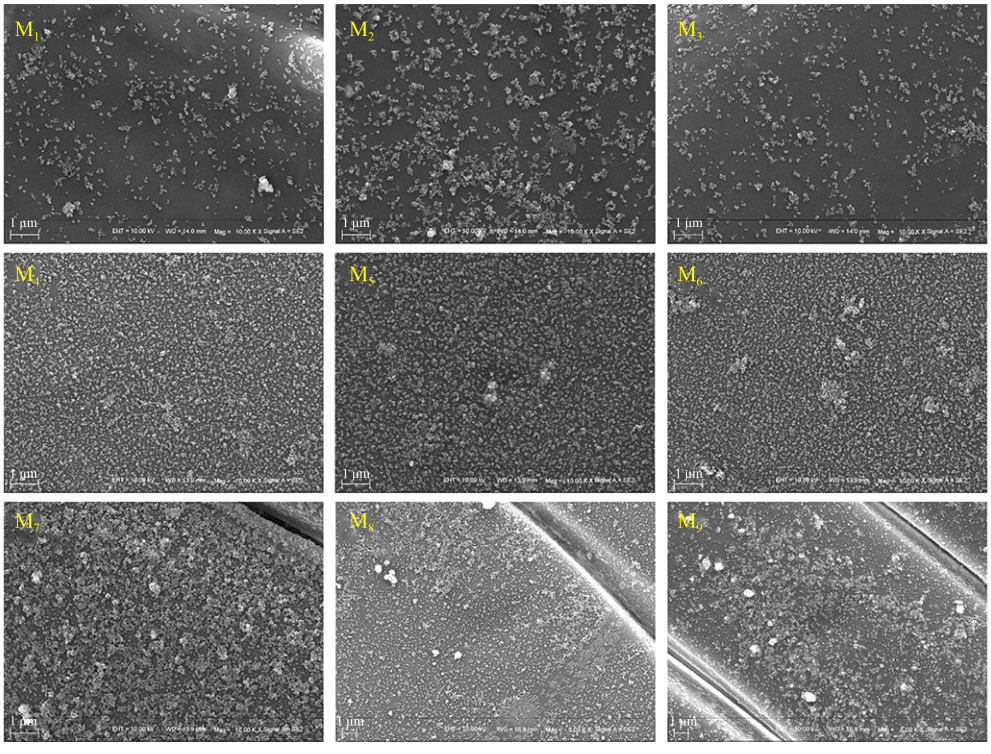

Fig. 2 SEM images of modified membrane M_1–M_9.

became much rougher. It can be concluded that the optimal concentration of TiO_2 was 0.25 g·L^{-1}, which is consistent with the CA's optimal preparation condition. The membrane prepared under optimal conditions is marked as M_B in the following figure.

3.2 Membrane characterization

Figure 3 shows the surface morphology of the polyester base material before and after modification. Figures 3(a, e) depict that the unmodified membrane exhibited clean and smooth fibres. Following the modification of individual TiO_2, TiO_2 nanoparticles were anchored onto the surface (Figures 3(b, e)). Because PFOTS molecular layer cannot be observed in the SEM images, no noticeable difference was present between the TiO_2-loaded membrane (Figures 3(b, e)) and TiO_2 + PFOTS-loaded membrane, M_B (Figures 3(c, f)).

EDS was used to confirm the membrane's chemical composition. Figure 4 shows the chemical composition of M_0 and M_B. Only carbon and oxygen were detected from the M_0, containing 80.89 wt % carbon and 19.11 wt %

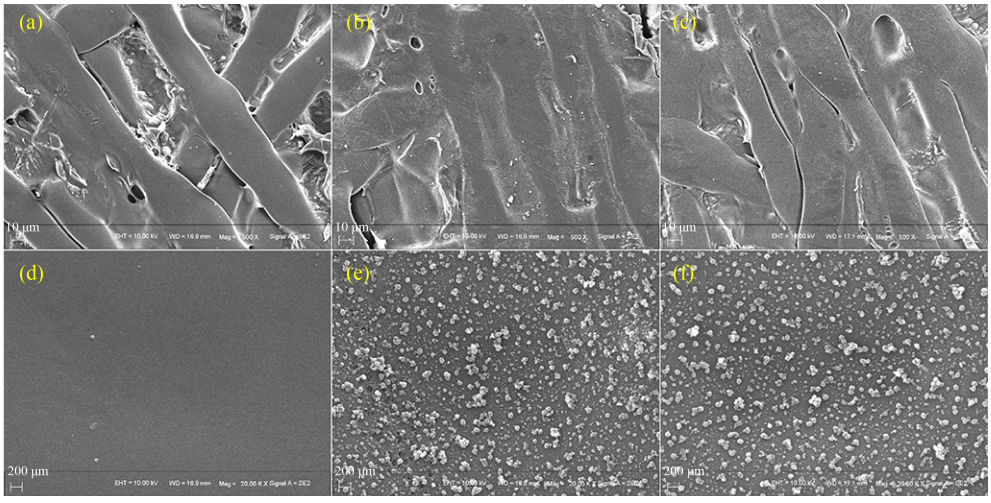

Fig. 3 Low-resolution SEM images of (a) M_0, (b) TiO_2-loaded membrane and (c) TiO_2 + PFOTS-modified membrane, and high-resolution SEM images of (d) M_0, (e) TiO_2 loaded membrane and (f) TiO_2 + PFOTS-modified membrane.

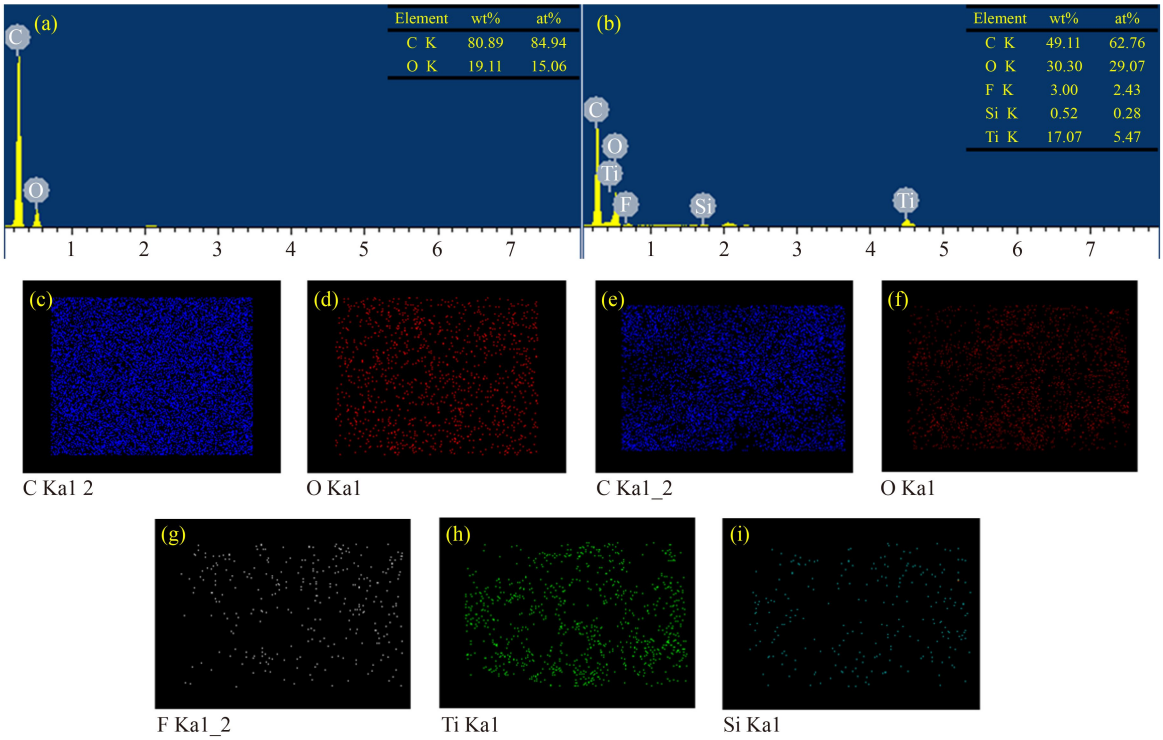

Fig. 4 EDS images of the (a) unmodified membrane, (b) TiO_2 + PFOTS-modified membrane. (c, d) EDS mapping images of C, O elements on the unmodified membrane, and (e–i) C, O, F, Ti, Si elements on the modified membrane.

oxygen. Large amounts of titanium, silicon and fluorine were observed on M_B, indicating that M_B has been successfully modified. Moreover, M_B's corresponding EDS mapping images in Figs. 4(e–i) show that C, O, F, Si and Ti elements were evenly distributed on M_B, indicating the full and uniform coverage of TiO_2 nanoparticles grafted with fluorine polymers on M_B. Consequently, the large rough structures combined with pretty low surface energy, produced by the C–F bond in PFOTS, could provide the MB surface with a large area to trap air but repel water, imparting the modified fabric with excellent hydrophobicity.

Figure 5 shows that the change of surface groups in the membrane can be distinguished from FTIR and XPS spectra. In the FTIR spectra (Fig. 5(a)), the new vibration bands at 1296 and 1278 cm^{-1} in M_B were assigned to the C–F of PFOTS [36], indicating PFOTS was successfully attached to the surface of the membrane. Characteristic peaks of C 1s and O 1s were detected in the XPS survey spectra of all membranes (Fig. 5(b)). Following the modification of TiO_2 and PFOTS, an obvious signal of F KLL, F 1s, Ti 2p and Si 2p was found at around 835, 689, 463 and 103 eV, respectively. Moreover, the high-resolution C 1s spectrum of M_0 (Fig. 5(c)) revealed three signals at 284.8, 286.4, and 288.8 eV, which were mainly assigned to the C–C/C–H, C–O–C and C=O/O–C=O groups, respectively. Compared with the high-resolution C 1s spectrum of the M_0, there were two new signals at 291.3 and 293.6 eV, which were mainly assigned to the CF_2 and CF_3 groups, respectively, in PFOTS. The FTIR and XPS spectra results also demonstrated the successful introduction of TiO_2 and PFOTS on the membrane surface.

The *CA* is an important parameter for reflecting the wettability of membranes, which considerably influences the pure water flux. Figure 6 shows the *CA* of the modified membrane (M_B) with various solutions of water (dyed with methylene blue), milk, juice, vinegar and tea, etc. The *CA* of M_B reached 135.2° ± 0.3°, which was significantly greater than the unmodified membrane (M_0) with 67.2° ± 1.9°, showing a better hydrophobic performance. The modified membrane demonstrated better hydrophobicity because PFOTS generated long-chain fluorine molecules on the surface. The increasing surface roughness was also beneficial to the hydrophobic property of the membrane, which is consistent with SEM [37]. PFOTS have low surface energy. The tightly bonded non-bonded electron pairs in C–F bonds are not easily polarized and hinder hydrogen bonds' interactions and dispersions with polar and non-polar liquids. This non-attractive behaviour increases with the degree of fluorine substitution for each carbon centre (i.e., $CF_3 > CF_2 > CF$) and depends on the length of the perfluoroalkyl chain [38].

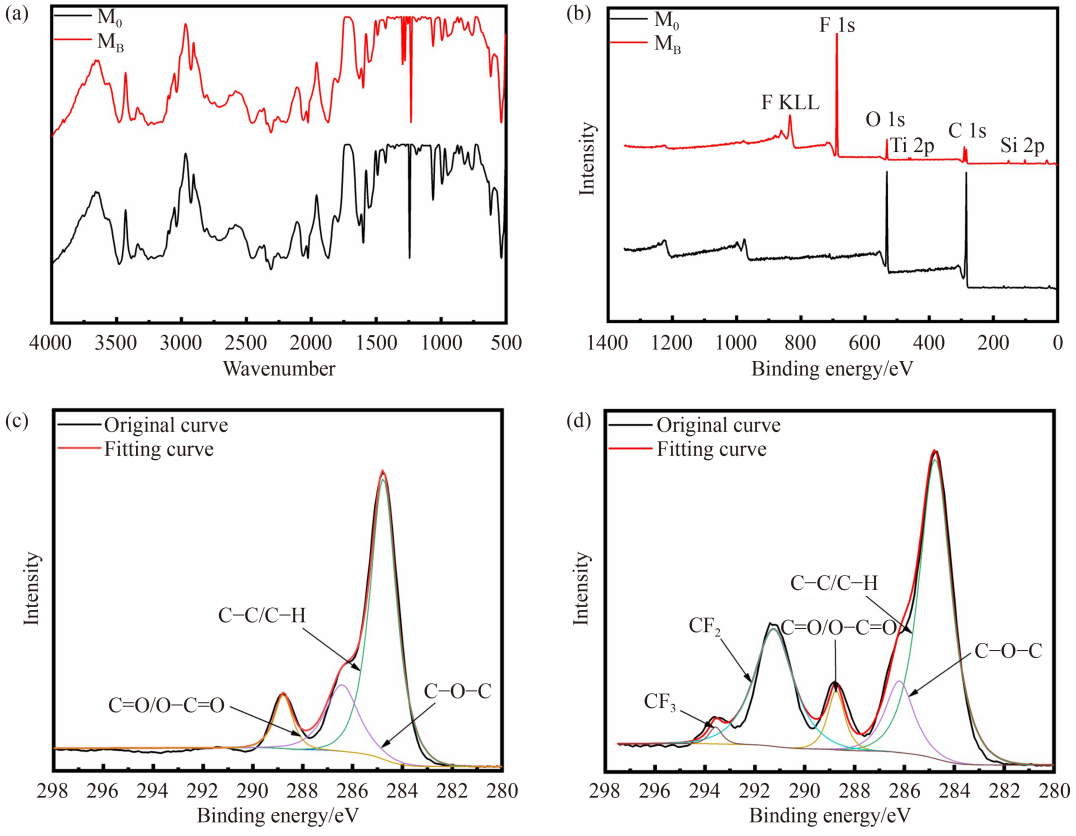

Fig. 5 Physicochemical characterization: (a) FTIR spectra of the pristine (M_0) and modified membrane (M_B); (b) XPS spectra of the pristine (M_0) and modified membrane (M_B); high-resolution C 1s spectrum of (c) M_0 and (d) M_B.

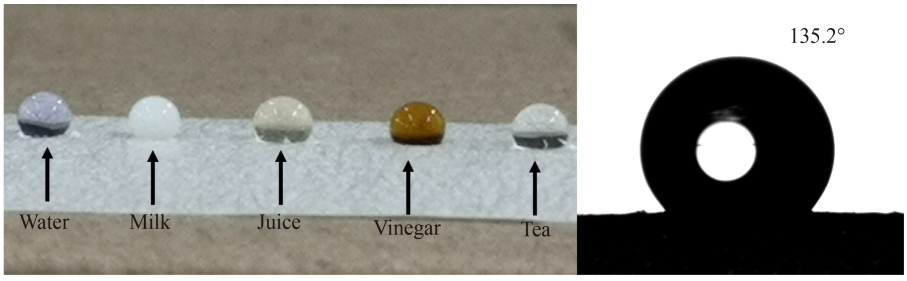

Fig. 6 Wettability of the hydrophobic coating with various solutions and *CA* of M_B.

3.3 Oil–water separation

The dead-end filter device is used to perform the oil–water separation test of the modified membrane under gravity. Oil–water separation tests were conducted in three systems: light oil/water (petroleum ether/water) system, heavy oil/water (carbon tetrachloride/water) system and light oil/water/heavy oil (petroleum ether/water/carbon tetrachloride) system. Figure 7 shows the results of the oil–water separation experiment.

Because of the hydrophobicity of the modified membrane, water could not pass through after contacting the modified membrane and not achieve oil–water separation for the petroleum ether/water (Fig. 7(a))

Fig. 7 The oil/water separation process of (a) petroleum ether/water system; (b) carbon tetrachloride/water system; (c) petroleum ether water/carbon tetrachloride system, the water is blue (methyl blue dyeing), and the oil is orange-red (Sudan III dyeing).

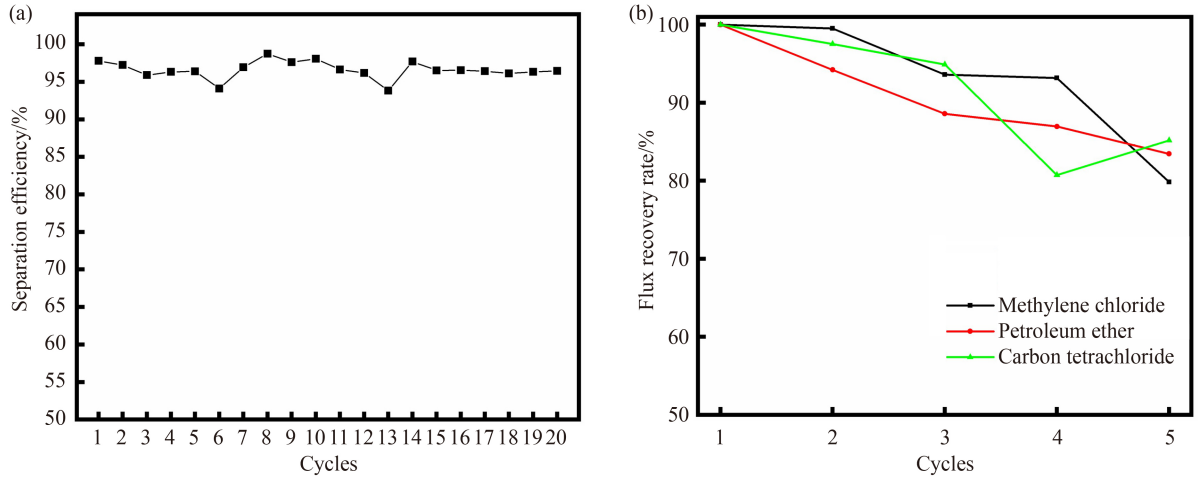

Fig. 8 (a) Separation efficiencies of M_B for carbon tetrachloride/ water system with different cycles. (b) The FRR of M_B for three oil testing systems with different cycles.

system. Carbon tetrachloride could normally pass in the carbon tetrachloride/water (Fig. 7(b)) system. The water is completely trapped on the membrane. In the petroleum ether/water/carbon tetrachloride (Fig. 7(c)) system, the water was completely trapped on the surface of the modified membrane after carbon tetrachloride passed through the modified membrane. In contrast, petroleum ether could not pass through because it floats on the water's surface.

Carbon tetrachloride and carbon tetrachloride/water systems were selected to test the modified membrane's permeation flux and separation efficiency. The oil flux of M_0 is only 157.89 ± 3.30 $L \cdot m^{-2} \cdot h^{-1}$, which is lower than the oil flux of M_B of 242.34 ± 9.63 $L \cdot m^{-2} \cdot h^{-1}$. This result indicated that the modified membrane exhibited a significant increase in oil flux. Furthermore, the oil–water separation efficiency of the modified membrane also showed an apparent increase from 0 to 97.8%.

The stability measurement was conducted to evaluate the sustainability of the modified membrane (Fig. 8). During the 20 cycles test, for the carbon tetrachloride/water system, the oil–water separation efficiency was kept at a high level of 96% for the carbon tetrachloride/water system. The modified membrane exhibited a good FRR for different oil testing systems, such as methylene chloride, petroleum ether, and carbon tetrachloride. Figure 8(b) shows that the oil FRR exhibited about 20% decrease after five cycles.

4 Conclusions

In this work, a simple and efficient surface modification strategy, TiO_2 and PFOTS deposition, was successfully used to modify the base nonwoven fabric layer of the wasted RO membrane to improve its hydrophobic property. The orthogonal experiment revealed the following optimum conditions of TiO_2 mass concentration, PFOTS volume concentration, and the deposition times of TiO_2 and PFOTS: 0.25 $g \cdot L^{-1}$ of TiO_2 mass concentration, 15 min of TiO_2 deposition time, 0.75 $mL \cdot L^{-1}$ of PFOTS volume concentration and 10 min of PFOTS deposition time, respectively. The optimally modified membrane showed good hydrophobicity and oil–water separation performance, the *CA* could reach 135.2° ± 0.3° and the oil–water separation performance was as high as 97.8%. This outcome provides a consistently high oil filtrate FRR (> 80%) in various oil systems and excellent oil–water separation performance (> 96%) in treating carbon tetrachloride/water system during the 20 cycles of testing. In summary, this study developed a durable and sustainable membrane for oil–water separation and provided an effective method for the reutilization of wasted RO membrane.

Acknowledgements We gratefully acknowledge the financial support from the National Natural Science Foundation of China (Grant No. 21576205), the Tianjin Natural Science Foundation (Grant No. 18JCTPJC48600), and the Training Project of Innovation Team of Colleges and Universities in Tianjin (Grant No. TD13-5020).

Electronic Supplementary Material Supplementary material is available in the online version of this article at https://dx.doi.org/10.1007/s11705-022-2200-0 and is accessible for authorized users.

References

1. Stefano C, Mirko F, Francesca M, Enrico D. A review on membrane distillation in process engineering: design and exergy equations, materials and wetting problems. Frontiers of Chemical Science and Engineering, 2022, 16(5): 592–613
2. UNESCO. UN-Water. United Nations World Water Development Report 2020: Water and Climate Change. Paris: UNESCO, 2020: 46–57
3. Lejarazu-Larraaga A, Molina S, Ortiz J M, Riccardelli G, García-

Calvo E. Influence of acid/base activation treatment in the performance of recycled electromembrane for fresh water production by electrodialysis. Chemosphere, 2020, 248: 126027
4. Jeffrey J M, Gina M V. Framework for Direct Potable Re-use. Alexandria: Water Reuse Research Foundation, 2015
5. Guo H, Li X H, Yang W L, Yao Z K, Mei Y, Peng L E, Yang Z, Shao S L, Tang C Y. Nanofiltration for drinking water treatment: a review. Frontiers of Chemical Science and Engineering, 2022, 16(5): 681–698
6. García-Pachecoa R, Landaburu-Aguirrea J, Terrero-Rodríguezc P, Camposc E, Molina-Serranoc F, Rabadána J, Zarzoc D, García-Calvo E. Validation of recycled membranes for treating brackish water at pilot scale. Desalination, 2018, 433: 199–208
7. Zhao Y, Qiu Y B, Mamrol N, Ren L F, Li X, Shao J H, Yang X, Bart V D B. Membrane bioreactors for hospital wastewater treatment: recent advancements in membranes and processes. Frontiers of Chemical Science and Engineering, 2022, 16(5): 634–660
8. Chen R Z, Dong X F, Ge Q C. Lithium-based draw solute for forward osmosis to treat wastewater discharged from lithium-ion battery manufacturing. Frontiers of Chemical Science and Engineering, 2022, 16(5): 755–763
9. Jorge S S, Alberto B, Raquel G P, Junkal L A, Eloy G C. Prospective life cycle assessment and economic analysis of direct recycling of wasted reverse osmosis membranes based on geographic information systems. Journal of Cleaner Production, 2021, 282: 124400
10. Liyanaarachchi S, Shu L, Muthukumaran S, Jegatheesan V, Baskaran K. Problems in seawater industrial desalination processes and potential sustainable solutions: a review. Reviews in Environmental Science and Biotechnology, 2014, 13(2): 203–214
11. Ismail A F, Padaki M, Hilal N, Matsuura T, Lau W J. Thin film composite membrane: recent development and future potential. Desalination, 2015, 356: 140–148
12. Shenvi S S, Isloor A M, Ismail A F. A review on RO membrane technology: developments and challenges. Desalination, 2015, 368: 10–26
13. Greenlee L F, Lawler D F, Freeman B D, Marrot B, Moulin P. Reverse osmosis desalination: water sources, technology, and today's challenges. Water Research, 2009, 43(9): 2317–2348
14. Yearbook I D A. Topsfield. Water Desalination Report, 2018–2019, 2019
15. Ziolkowska J R. Is desalination affordable?—regional cost and price analysis. Water Resources Management, 2015, 29(5): 1385–1397
16. Junkal L A, Raquel G P, Serena M, Laura R S, Javier R, Eloy G C. Fouling prevention, preparing for re-use and membrane recycling. Towards circular economy in RO desalination. Desalination, 2016, 393: 16–30
17. Jorge S S, Raquel G P, Junkal L A, Eloy G C. Recycling of wasted reverse osmosis membranes: comparative LCA and cost-effectiveness analysis at pilot scale. Resources, Conservation and Recycling, 2019, 150: 104423
18. Li W C, Tse H F, Fok L. Plastic waste in the marine environment: a review of sources, occurrence and effects. Science of the Total Environment, 2016, 566: 333–349
19. Raquel G P, Junkal L A, Amaia L L, Laura R S, Serena M, Thomas R, Eloy G C. Free chlorine exposure dose (ppm·h) and its impact on RO membranes ageing and recycling potential. Desalination, 2019, 457: 133–143
20. Paula E C D, Amaral M C S. Extending the life-cycle of reverse osmosis membranes: a review. Waste Management & Research, 2017, 35(5): 456–470
21. Goosen M F A, Sablani S S, Al-Hinai H, Al-Obeidani S, Al-Belushi R, Jackson D. Fouling of reverse osmosis and ultrafiltration membranes: a critical review. Separation Science and Technology, 2005, 39(10): 2261–2297
22. Mohammad R M, Arto P, Mehrdad H, Jonni A, Mika M. Wasted RO membranes recycling: re-use as NF membranes by polyelectrolyte layer-by-layer deposition. Journal of Membrane Science, 2019, 584: 300–308
23. Jesús M L, Lucía N R, Jorge S S, Serena M, Rehab E S. Recycled desalination membranes as a support material for biofilm development: a new approach for microcystin removal during water treatment. Science of the Total Environment, 2019, 647: 785–793
24. Jesús M L, Serena M. Optimization of recycled-membrane biofilm reactor (R-MBfR) as a sustainable biological treatment for microcystins removal. Biochemical Engineering Journal, 2020, 153: 107422
25. Will L, Zenah B H, Marlene J C, Mikel D, Greg L, Bradley P L, Pierre L C. Towards new opportunities for re-use, recycling and disposal of used reverse osmosis membranes. Desalination, 2012, 299: 103–112
26. Eduardo C D P, Míriam C S A. Environmental and economic evaluation of wasted reverse osmosis membranes recycling by means of chemical conversion. Journal of Cleaner Production, 2018, 194: 85–93
27. Hou L, Zhang Y Q. Research status on the system of spiralwound reverse osmosis membrane module for sea water desalination. Technology of Water Treatment, 2015, 41(10): 21–25
28. Goh P S, Wong K C, Wong T W, Ismail A F. Surface-tailoring chlorine resistant materials and strategies for polyamide thin film composite reverse osmosis membranes. Frontiers of Chemical Science and Engineering, 2022, 16(5): 564–591
29. Plopeanu M C, Dascalescu L, Yahiaoui B, Antoniu A, Hulea M, Notingher P V. Repartition of electric potential at the surface of nonwoven fabrics for air filtration. IEEE Transactions on Industry Applications, 2012, 48(3): 851–856
30. Anandjiwala R D, Boguslavsky L. Development of needle-punched nonwoven fabrics from flax fibers for air filtration applications. Textile Research Journal, 2008, 78(7): 614–624
31. Sugioka M, Yoshida N, Yamane T, Kakihana Y, Higa M, Matsumura T, Sakoda M, Iida K. Long-term evaluation of an air-cathode microbial fuel cell with an anion exchange membrane in a 226 L wastewater treatment reactor. Environmental Research, 2022, 205: 112416
32. Zhao P, Qin N, Ren C L, Wen J Z. Surface modification of polyamide meshes and nonwoven fabrics by plasma etching and a PDA/cellulose coating for oil/water separation. Applied Surface Science, 2019, 481: 883–891

33. Yuan Z S, Ke Z W, Qiu Y H, Zheng L J, Yang Y, Gu Q S, Wang C Y. Prewetting polypropylene-wood pulp fiber composite nonwoven fabric for oil–water separation. ACS Applied Materials & Interfaces, 2020, 12(41): 46923–46932
34. Babiker D M D, Zhu L P, Yagoub H, Lin F, Altam A A, Liang S M, Jin Y, Yang S G. The change from hydrophilicity to hydrophobicity of HEC/PAA complex membrane for water-in-oil emulsion separation: thermal versus chemical treatment. Carbohydrate Polymers, 2020, 241: 116343
35. Sun F, Li T T, Zhang X Y, Shiu B C, Zhang Y, Lou C W, Lin J H. Preparation and oil–water separation evaluations of polypropylene/low-melt-point polyester composites reinforced by thermal bonding and one-step solution immersion. Polymer International, 2020, 69(9): 752–762
36. Pandit S K, Tudu B K, Mishra I M, Kumar A. Development of stain resistant, superhydrophobic and self-cleaning coating on wood surface. Progress in Organic Coatings, 2020, 139: 105453
37. Nanda D, Swetha T, Varshney P, Gupta P K, Mohapatra S S, Kumar A. Temperature dependent switchable superamphiphobic coating on steel alloy surface. Journal of Alloys and Compounds, 2017, 727: 1293–1301
38. Ma Z, Shu G M, Lu X L. Preparation of an antifouling and easy cleaning membrane based on amphiphobic fluorine island structure and chemical cleaning responsiveness. Journal of Membrane Science, 2020, 611: 118403